RSC Advances

PAPER

View Article Online
View Journal | View Issue



Cite this: *RSC Adv.*, 2022, **12**, 33751

# Waste acrylonitrile butadiene styrene (ABS) incorporated with polyvinylpyrrolidone (PVP) for potential water filtration membrane

Syarifa Nur'aini,[a] Akmal Zulfi,*[b] Bagas Haqi Arrosyid,[a] Ande Fudja Rafryanto,[a] Alfian Noviyanto,*[ac] Dian Ahmad Hapidin,[d] Dafit Feriyanto,[c] Kurniawan Eko Saputro,[a] Khairurrijal Khairurrijal[d] and Nurul Taufiqu Rochman[e]

Acrylonitrile butadiene styrene (ABS) is one of the most common fused-filament feedstocks for 3D printing. The rapid growth of the 3D printing industry has resulted in huge demand for ABS filaments; however, it generates a large amount of waste. This study developed a novel method using waste ABS to fabricate electrospun nanofiber membranes (ENMs) for water filtration. Polyvinylpyrrolidone (PVP) was employed to modify the properties of waste ABS, and the effect of PVP addition in the range of 0–5 wt% was investigated. The results showed that adding PVP increased the viscosity and surface tension but decreased the conductivity of the precursor solution. After electrospinning, PVP could reduce the number of beads, increase the porosity and fiber diameter, and improve the wettability of the fabricated fibers. Moreover, the bilayer of ABS ENMs achieved a high flux value between 2951 and 48 041 L $m^{-2}$ $h^{-1}$ and a high rejection rate of 99%. Our study demonstrates a sustainable strategy to convert waste plastics to inexpensive materials for wastewater treatment membranes.

Received 21st September 2022
Accepted 18th November 2022

DOI: 10.1039/d2ra05969j

rsc.li/rsc-advances



## Introduction

Acrylonitrile butadiene styrene (ABS) is a thermoplastic polymer consisting of 70–80% styrene–acrylonitrile copolymer (SAN) and 20–30% polybutadiene rubber.[1,2] Owing to its excellent heat resistance, glossy surfaces, high hardness, and easy processability,[3] ABS has been widely used as housing materials for automotive systems, air conditioners, computers, and electronic appliances.[3–7] Rapid technology development requires design freedom for customized parts; therefore, 3D printing has become popular for polymer fabrication in many fields.[8] This remarkable technology creates a high demand for filaments as feedstock, and ABS is one of the most common polymer feedstock.[9,10] The high demand for ABS filament also increases its waste. ABS waste is the major component of waste electrical and electronic equipment (WEEE).[11,12] The WEEE streams contributed to 20% of all plastic waste types and reached 53.6 million tons in 2019.[13] The common methods of plastic waste treatment include landfilling and incineration, which are not environmentally safe.[14] The landfill process may pollute groundwater, and the incineration of WEEE causes toxic dust containing heavy metals, dioxins, and other harmful substances.[15–17] Therefore, it is urgently required to develop a sustainable solution to recycle ABS waste.

Several studies have attempted to utilize ABS waste in higher-value products such as additive bitumen binders,[18] green catalysts for oil and metal recovery,[19] recycled filaments for reuse in 3D printing,[20] and epoxy materials.[4] Recently, ABS waste has been recycled into nanofiber membranes for air filtration.[21,22] Nanofiber membranes made from recycled ABS waste exhibited filtration efficiencies of approximately 95% for PM 2.5 because the interconnected pore structures and the large surface area were suitable for particle capture during gas filtration. Nanofiber membranes also have a unique pore structure, narrow pore size, and high selectivity,[23] which are ideal for water treatment and filtration.[24–28] Excellent performance has been achieved with an efficiency of 99.99% and a flux of 5000–35 000 L $m^{-2}$ $h^{-1}$.[29–32] However, to the best of the authors knowledge, there are no reports on recycling ABS waste into water filtration membranes.

Electrospinning is a well-known technique for fabricating nanofiber membranes from various polymers. This technique is versatile and has the ability to control nanofiber morphology by adjusting the solution and process parameters.[33] ABS nanofiber membranes have hydrophobic surfaces,[21,34] which are

[a]*Nano Center Indonesia, Jalan Raya PUSPIPTEK, South Tangerang, Banten 15314, Indonesia. E-mail: a.noviyanto@nano.or.id*

[b]*Research Center for Environmental and Clean Technology, National Research and Innovation Agency, Bandung Advanced Science and Creative Engineering Space (BASICS), Jl. Cisitu, Bandung 40135, Indonesia. E-mail: akmal.zulfi.m@brin.go.id*

[c]*Department of Mechanical Engineering, Mercu Buana University, Jl. Meruya Selatan, Kebun Jeruk, Jakarta 11650, Indonesia. E-mail: alfian.noviyanto@mercubuana.ac.id*

[d]*Department of Physics, Institut Teknologi Bandung, Jalan Ganesa 10, Bandung 40132, Indonesia*

[e]*Research Center for Metallurgy and Materials, National Research and Innovation Agency, South Tangerang, Banten 15314, Indonesia*

unfavorable for water filtration because they can increase energy consumption.[35] Therefore, water-soluble materials are often added to enhance the membrane flux. Polyvinylpyrrolidone (PVP) and polydopamine (PDA) increased the surface hydrophilicity and flux rate of the membranes.[36] Another study by Park *et al.* reported that the modification of a hydrophobic membrane with polyvinyl alcohol (PVA) could enhance membrane performance.[37]

The present work aimed to recycle ABS to electrospun nanofiber membranes (ENMs) for microfiltration in a 2500 ppm antacid solution. This study also investigated the surface modification of ENMs by blending waste ABS with PVP. Adding PVP is expected to improve the hydrophilicity of ENMs and enhance the permeate flux as well as filtration efficiency. The ENMs prepared with waste ABS in this study have comparable filtration performance to the membranes prepared using expensive polymers. In addition, recycling ABS waste has a positive impact on the environment.

## Experimental materials

ABS was obtained as 3D-printing filament waste from Shenzhen eSun Industrial Co. Ltd PVP ($M_w$ = 1 300 000) was purchased from Sigma-Aldrich. *N*,*N*-dimethylformamide (DMF) was used as the solvent (Sigma-Aldrich). In addition, commercial nonwoven polyethylene terephthalate (PET) was used as the substrate to deposit the nanofiber, and a commercial antacid was used as a particle model in the membrane performance test.

### Synthesis of ENMs

ABS filament waste was washed and cut into pieces to facilitate the subsequent dissolution process. ABS and PVP with various weight percentages were dissolved in DMF at 40–50 °C under magnetic stirring until the solution became homogeneous. A conductometer (Mettler Toledo, Seveneasy Conductivity, Switzerland), Fenske–Oswald viscometer (Fisher Scientific, 50 A643), and du Noüy ring tensiometer (Fisher) were used to measure the conductivity, viscosity, and surface tension of the precursor solutions, respectively. The measurements were performed at room temperature (25 ± 5 °C). Table 1 lists the weight percentages (wt%) of ABS and PVP used in each precursor solution and its measured conductivity, viscosity, and surface tension.

The precursor solution was loaded into a commercial syringe-fitted stainless-steel needle with an inner diameter of 0.7 mm. The filled syringe was controlled by a syringe pump at a constant rate of 0.3 mL hour$^{-1}$. The tip of the needle was connected to a high-voltage source operated at 12 kV. The distance between the needle tip and the drum collector was 12–15 cm. The drum collector was grounded and rotated to deposit the spun fibers. To compile the nanofibers easily, the drum collector was also wrapped with nonwovens. The apparatus was set up in a horizontal-spinning configuration at room temperature (25 ± 5 °C) under a relative humidity of 60%. ENMs were continuously synthesized for 7 h to obtain nanofibers on an electrospinning apparatus (ILMI-N101, Integrated Laboratory of Materials and Instrumentation, ITB, Indonesia).

Table 1 Composition of polymers in the precursor solution and the solution properties

| Parameter/code | ABSP0 | ABSP1 | ABSP3 | ABSP5 |
|---|---|---|---|---|
| ABS (wt%) | 28 | 27 | 25 | 23 |
| PVP (wt%) | 0 | 1 | 3 | 5 |
| Viscosity (cP) | 153.91 | 384.82 | 858.12 | 1259.81 |
| Conductivity (μS) | 9.07 | 4.05 | 3.71 | 2.87 |
| Surface tension (dyne cm$^{-1}$) | 62.72 | 64.95 | 65.37 | 66.43 |

### Characterizations

X-ray diffraction (XRD, Rigaku MiniFlex 600) was used to measure the crystallinity of the ENMs at room temperature in the 2$\theta$ range of 5°–90°. The chemical bonds in the fiber were analyzed by Fourier transform infrared spectroscopy (FTIR, Thermo Scientific Nicolet iS10). The size and morphology of the ENMs were observed by scanning electron microscopy (SEM, Hitachi SU3500). Before SEM observation, the ENMs were coated with Au to enhance conductivity and minimize charging. The fiber size distribution was calculated based on 250 random fibers, while the diameter of the beads was estimated by measuring the length and width of the beads in the SEM images using the Image J software. The surface porosity was obtained by two-dimensional calculation on the SEM image, as described in a previous study.[38–40]

Because the ENMs are projected for water filtration, the water contact angle (WCA) is an important parameter to ensure hydrophilicity. Therefore, WCA was investigated using a contact angle apparatus (Nachriebe 320, Nachriebe). Water (5 μL) was used to create a droplet and the shape of the droplet on the membrane surface was captured using a camera, and the image was digitally processed using Image J software to obtain the WCA.

### Performance and filtration test

The performance of the ENMs was assessed using the flux value of pure water and the efficiency of particle rejection. Dead-end

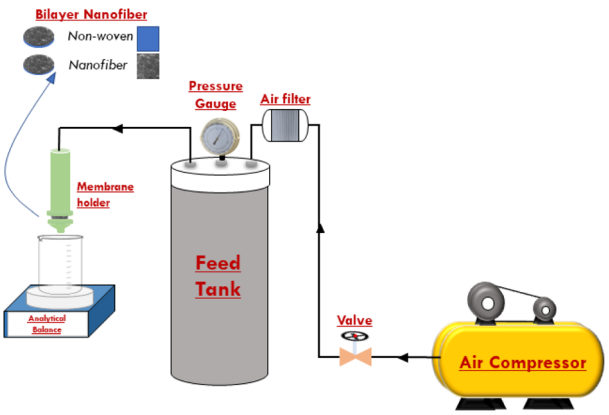


Fig. 1 Schematic of ENMs performance evaluation system.

flux was evaluated using a system containing a compressors, valves, prefilters, low-pressure regulators, membrane holders, and an analytical balance (Fig. 1).[36,40] The pressure for the pure water flux (PWF) test was controlled between 0.025 and 0.1 bar, while the pressure for filtration evaluation was 0.025 bar. Low pressure was applied in the microfiltration process.[28] Pressurized clean air flowed through the ENMs to obtain the permeate volume. The bilayer nanofiber is an assembly of two pieces of ENMs and substrates arranged alternately. The PWF value indicated the maximum amount of fluid that was streamed through the ENMs. The higher the flux value, the less energy consumed.[41–43] The flux value ($J$) can be expressed by eqn (1).

$$J = \frac{V}{A \cdot t} \quad (1)$$

where $V$ is the permeate volume ($m^3$), $A$ is the membrane surface area ($m^2$), $t$ is the time used in the filtration process (s).[32] In addition to the PWF value, the ability of the ENMs to filter particles was assessed using an antacid solution (2500 ppm) streamed through the membrane. Because particle size was essential for defining the type of filtration, the mean particle size of the antacid was measured using a particle size analyzer (Beckman Coulter, Delsa Nano C). Fig. 2 shows the narrow distribution of antacid particles with a polydispersity index of 0.28, and the mean particle was 1174.3 nm.[44]

The feed and permeate concentrations were measured using a UV/Vis spectrophotometer (Labtron LUS-B13). The concentration was determined based on a calibration curve.[45] The concentrations used for calibration were 2500, 1875, 1250, 625, 317, and 0 ppm. The permeate concentration was derived from the calibration curve. The retention ratio (%) was calculated using eqn (2):[46,47]

$$\text{Rejection } (\%) = \left(1 - \frac{C_{\text{permeate}}}{C_{\text{feed}}}\right) \quad (2)$$

where $C_{\text{feed}}$ and $C_{\text{permeate}}$ are the concentrations of the feed and permeate, respectively.

# Results and discussion

## Nanofiber characterization

Nanofibers were successfully prepared using the solution of 23–28 wt% ABS waste and 1–5 wt% PVP. The XRD patterns of ABSPs (Fig. 3) agreed with the characteristics of amorphous materials.[48] ABSP0 had a broad peak between 10° and 30° similar to the pure ABS reported in a previous study.[49] However, the peak intensity of the ABSP0 was higher. Some reports attributed the high intensity to the molding process and the intermolecular hydrogen bonding.[50,51] Nevertheless, the XRD pattern of ABSP0 was in agreement with the study using ABS as an amorphous feedstock polymer.[9,52] For comparison, the ENM with 10 wt% PVP was prepared to show the typical peak of pure PVP. Therefore, it can be understood the difference in the XRD patterns of ABSP1, ABSP3, and ABSP5 are due to the addition of PVP. In line with the previous study, the addition of other polymer with high molecular weight will decrease the intensity of XRD pattern.[53]

Fig. 4 shows the FTIR spectra of the ENMs. ABS was formed by polymerizing three monomers, *i.e.*, acrylonitrile, polybutadiene, and styrene. The spectra of ABS waste were similar to the previous report.[54,55] The peak at 3000–3100 $cm^{-1}$ was the absorption of asymmetric C–H aromatic bonds in styrene compounds, while the peak at 2800–3000 $cm^{-1}$ corresponded to the aliphatic C–H bond, and that at 2237 $cm^{-1}$ was the deformation of nitrile C≡N bonds. The C=C aromatic double bond stretching vibration was found at 1602 $cm^{-1}$. The peaks between 1495 and 1452 $cm^{-1}$ corresponded to the stretching of C–C in the aromatic ring, and the stretching of unsaturated C=C in polybutadiene. The bending C–H in-plane and (mono)-substituted out-of-plane vibrations were at 1074 and 1024 $cm^{-1}$ and 758 and 699 $cm^{-1}$, respectively. In our ABS waste, a carbonyl (C=O) stretching peak was observed at 1736 $cm^{-1}$ because of the oxidation during its usage and application.[4] The spectral peak of the pure PVP was in line with previous studies. The peak at 3464 $cm^{-1}$ was related to the stretching of

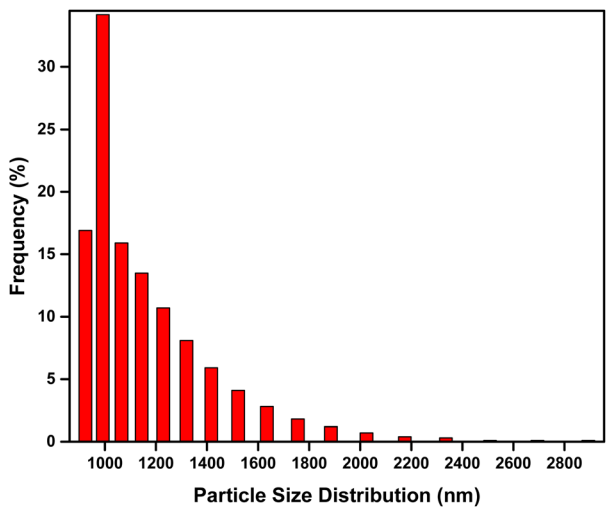


Fig. 2 Diameter distribution of antacid as a particle model.

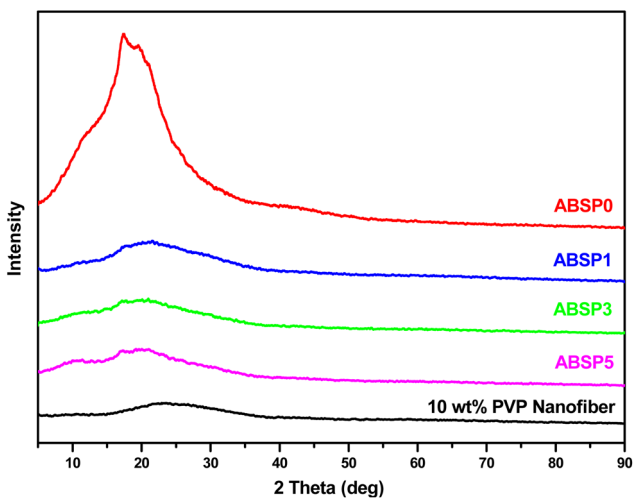


Fig. 3 XRD patterns of ENMs.

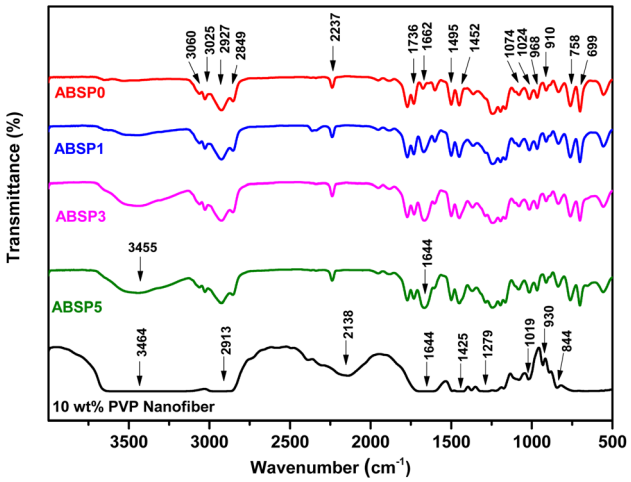


Fig. 4 FTIR Spectra of ENMs.

a hydroxyl group (hydrogen bonding). The peaks at 2913 $cm^{-1}$, 1644 $cm^{-1}$, 1425 $cm^{-1}$, and 1279 $cm^{-1}$ were assigned to the asymmetric $CH_2$ stretching, carbonyl group C=O, bending of C–H bond, C–N bond stretching, respectively. The peaks at 1019 $cm^{-1}$, 930 $cm^{-1}$, and 844 $cm^{-1}$ were attributed to the C–C bending. In the spectra of ABSPs, sharp peaks at 3455 $cm^{-1}$ and 1644 $cm^{-1}$ were observed due to the stretching of the hydrogen bonding (O–H) and carbonyl group (C=O), respectively. The reaction might occur between the C=O groups in the pyrrolidone ring and the hydrocarbons from polybutadiene or benzene compound[36] to form O–H and C=O bonds. DMF as a solution was not detected in the spectra of all samples, confirming that the solvent was completely evaporated.[56]

The SEM morphology of the ENMs (Fig. 5) shows the formation of bead nanofibers. A similar bead nanofiber was reported by Jiang *et al.* when 15 wt% of ABS in DMSO and $CHCl_3$ was used for electrospinning. The same method generated bead-free nanofiber when the ABS content was increased to 20–25 wt%.[34] Bead-free ABS nanofibers were obtained by mixing the solvent (DMF and THF) at a ratio of 9 : 1, as reported by Moradi *et al.*[57] Zulfi *et al.* prepared bead-free nanofibers from 30 wt% of ABS waste.[21] Therefore, the formation of bead nanofibers in this study was more likely due to the low concentration of ABS waste. Moreover, the source of ABS, solvent, and other additives might influence the formation of bead nanofiber.

Interestingly, the total number of beads was closely related to the weight percentage of PVP. For instance, the total number of beads for ABSP0, ABSP1, ABSP3, and ABSP5 were ~643, ~550, ~454, and ~262, respectively. PVP increased the viscosity of the precursor solution and improved jet stability, resulting in a decrease in bead formation. Moreover, the average bead diameter reduced with increasing PVP content. The average bead diameters of the ABSP0, ABSP1, ABSP3, and ABSP5 ENMs were 5.832, 5.382, 3.485, and 3.137 μm, respectively (Fig. 6). In addition to decreasing the number and size of the beads, PVP changed the beads from spherical to elongated shapes.[58] In this study, the shape change was not evident, and the coefficient of variance (CV) of the size was >0.3, suggesting the uniformity of beads or fibers.[59] The small number of beads in ABSP5 indicated that the size of the beads changed from large to small, eventually forming bead-free fibers. As shown in Table 1, a higher PVP content in the solution increased the viscosity and surface tension, and reduced the conductivity. This result is in agreement with published reports that showed bead-free fibers with higher PVP content.[60–62] However, the dependence of surface tension on the formation of beads was inconsistent in the literature. Almetwally *et al.* found that higher surface tension produced more beads on fiber.[63] However, Liu *et al.* reported that a high surface tension could yield a bead-free fiber.[64]

Fig. 7 shows the distribution of fiber diameters when different contents of PVP were added. The mean fiber diameters of the ABSP0, ABSP1, ABSP3, and ABSP5 ENMs were 108.46, 136.39, 173.71, and 216.64 nm, respectively. The fiber diameter increased with PVP, as reported previously.[65] The fiber diameters of ABSP3 and ABSP5 were considered a homogeneous

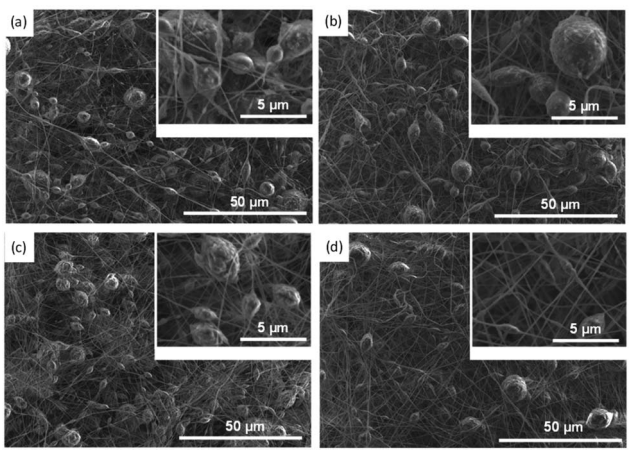


Fig. 5 SEM images of ENMs (a) ABSP0, (b) ABSP1, (c) ABSP3, and (d) ABSP5.

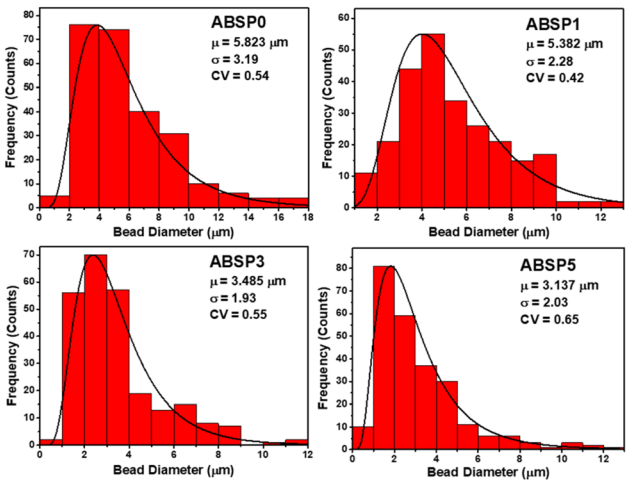


Fig. 6 Distribution of beads diameter based on the SEM images in Fig. 5.

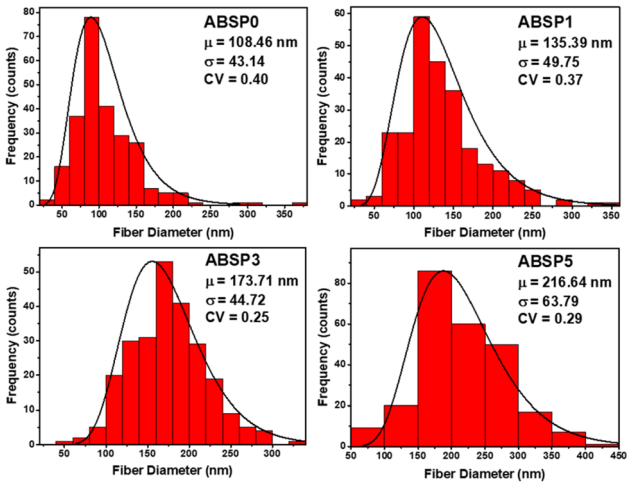


Fig. 7 Distribution of fiber diameter based on the SEM images in Fig. 5.

distribution, characterized by CV < 0.3. In contrast, the CV values of ABSP0 and ABSP1 were 0.37 and 0.4, respectively, implying an inhomogeneous fiber size. As shown in Table 1, the conductivity of the solution decreased with PVP; therefore, the thin fiber of ABSP0 was due to the high conductivity of the solution, consistent with a previous report that high conductivity generated thin fibers.[27]

The morphology of the ENMs also influenced the surface porosity. A high PVP concentration was reported to increase the porosity, which agreed with the present study that the porosities of ABSP1, ABSP3, and ABSP5 increased from 64.18, 70.33, to 71.78%, respectively. Porosity was more likely to be affected by the size of the fiber rather than the size of the bead. ABSP5 had a small bead diameter; however, the fiber diameter increased by a factor of two or more, resulting in its high porosity (71.78%). Comparatively, despite the large bead diameter of ABSP0, its porosity was only 65.23% owing to the small fiber diameter.

Fig. 8 shows the WCA of the ENMs that represent the hydrophilicity of membrane.[66] The two mechanisms of water passing through the membrane are (1) water penetrates the porous membranes and (2) water seeps into the membranes. As mentioned above, PVP is a water-soluble material;[67,68] thus, a high PVP content will increase the permeability of the membrane. Therefore, it was evident that the lowest WCA was found in ABSP5. Moreover, ABSP5 had more pores than the others, making it easier for water to pass through.[48] The average WCAs of ABSP0, ABSP1, ABSP3, and ABSP5 were 131.97°, 129.09°, 85.48°, and 53.40°, respectively, as shown in Fig. 8. It should be noted that ABSP0 was hydrophobic, consistent with previous studies.[21,34] Although PVP was water-soluble, adding 1 wt% PVP into ABS did not change the WCA. The WCA of ABS was reduced by adding at least 3 wt% of PVP. The ABSP3 had a WCA of 85.48° and could be categorized as hydrophilic, as well as ABSP5 which had WCA of 53.40°. Hydrophilic behavior is characterized by WCA < 90°.[69]

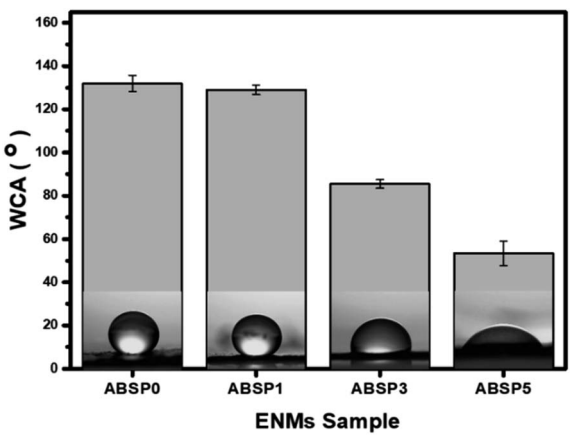


Fig. 8 Water contact angle measurement of ENMs.

## ENMs performance

Before the microfiltration test, the PWF values of the ENMs were examined to define the volume of permeate per unit time and the transmembrane pressure. The surface area directly in contact with the pure water and feed solution was 17.14 $cm^2$.

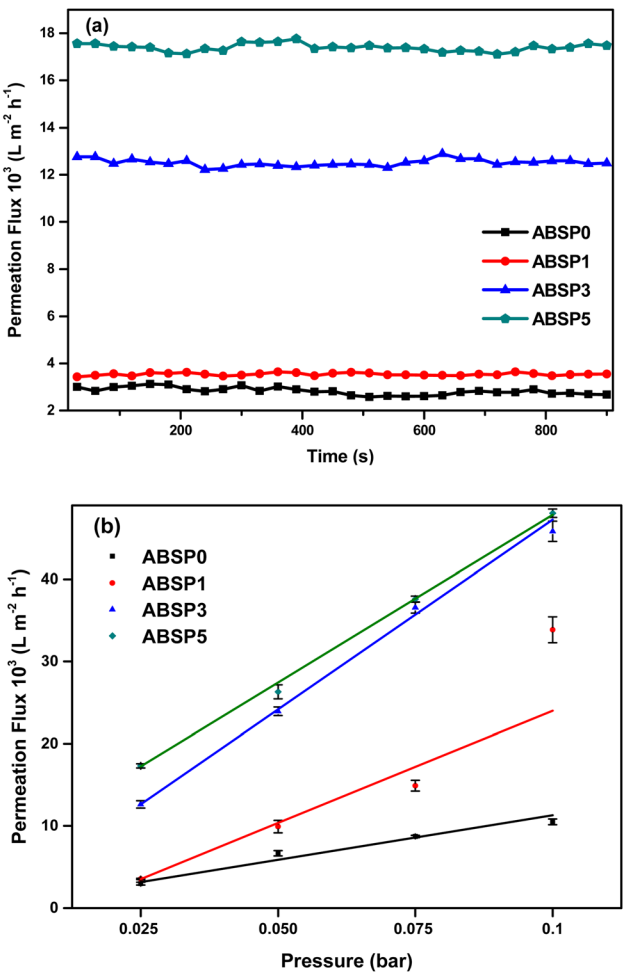


Fig. 9 Performance evaluation of ENMs (a) permeation flux at a fixed pressure (0.025 bar), and (b) permeation flux as a function of pressures.

The energy consumption was estimated for the permeate to pass through the membranes (permeability). Fig. 9(a) presents the PWF values of the ENMs at a fixed pressure of 0.025 bar. Indeed, the PWF was in accordance with the wettability, as explained in the previous subsection of nanofiber characterization. ABSP0 and ABSP1 had similarly low PWF values because of the hydrophobic properties of the ENMs. ABSP3 had a higher PWF due to increased hydrophilicity, and the PWF was the highest for ABSP5 owing to its hydrophilic properties. As shown in Fig. 9(a), average PWF values for ABSP0, ABSP1, ABSP3, and ABSP5 were 2820.2 ± 159, 3538.3 ± 56, 12 512.5 ± 152, and 17 395 ± 163 L $m^{-2}$ $h^{-1}$, respectively. Fig. 9(b) shows that the PWF increased with increasing applied pressure. The fluid flowing through a porous medium in a low-pressure condition follows Darcy's law,[70] which is derived from the Navier–Stokes equation:[71]

$$J = \frac{K}{\mu}\frac{\Delta P}{\Delta x} \quad (3)$$

where $K$ is the permeability constant, $\Delta P$ is the differential pressure, $\mu$ is the dynamic viscosity, and $\Delta x$ is the membrane thickness. Thus, the permeation flux at various pressure was quite broad from 2951 to 48 041 L $m^{-2}$ $h^{-1}$, as shown in Fig. 9(b). High permeability is one of the essential requirements for high-performance membranes because it can reduce energy consumption and manufacturing costs.[72] In contrast, the appearance of beads increased the pressure drop, which was another reason for the decreased permeability of ENMs with a large number of beads.[73]

This study used microfiltration because the particle model size was between 900 and 2600 nm. Therefore, besides the suspended solid larger than 0.1 μm, the other contaminants, such as oil emulsion, bacteria, cells, and colloidal haze, will be suspended in the membrane.[74] Fig. 10(a) shows the permeability of the ENMs using the particle model of antacids (Fig. 2). The rejection rates of ABSP1, ABSP3, and ABSP5 were 99%. Hence, the permeate solutions of ABSP1, ABSP3, and ABSP5 were clear, as shown in Fig. 10(b). In contrast, the permeate solution of ABSP0 was turbid in Fig. 10(b), corresponding to a rejection rate of 83%. These results indicated the importance of adding PVP to enhance the permeability of ABS ENMs. To the best of our knowledge, adding PVP to ABS waste has rarely been reported, particularly for water filtration applications. Moreover, this study successfully modified the surface characteristics of ABS waste, changing it from hydrophobicity suitable for air filtration[21] to hydrophilicity with the addition of PVP. Although the porosity of ABSP0 was smaller than that of the other ENMs, the filtration ability was not solely dependent on porosity. For instance, ABSP0 had a porosity of 65.23% and a rejection rate of 83%. Meanwhile, the rejection rate of ABSP1 was 99%, despite its similar porosity to ABSP0 (64.18%). Therefore, it can be concluded that PVP enhances the applicability of ABS waste for water filtration.

Three mechanisms are involved in the filtration process, *i.e.*, sieving, adsorption, and cake formation. Sieving occurs first as larger particles are retained on the surface of the membranes. Smaller particles flow through the inner membrane and are adsorbed on the fiber surface. Lastly, the particles in the membrane pores are retained on the surface and form a cake layer.[75] In this study, the cake layer was formed in two-hour filtration with 2500 ppm feed solution and remove manually. From the SEM images of ABSP1 after the filtration process (Fig. 11), depth filtration was confirmed in ABSP1. This membrane first accumulated particles on the surface, then small particles remained in the inner layer, resulting in a clear permeate. It seemed the cake formation mainly occurred on the surface for ABSP1. A previous study reported that depth filtration in bead fibers would extend the lifetime of the membrane, whereas filtration onto the membranes had a short lifetime and high-pressure drop.[76] Recently, clean-up processes for depth

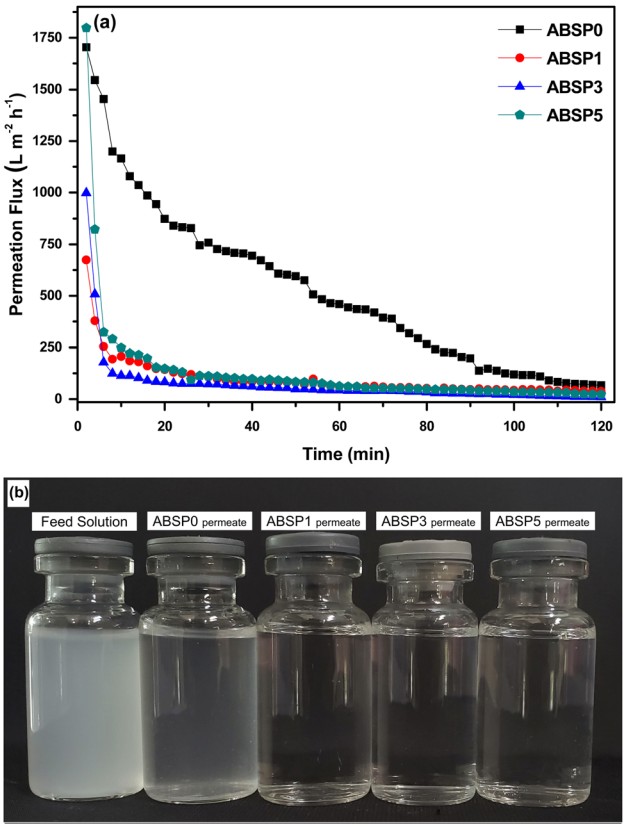


Fig. 10 (a) Permeation flux while filtration at 0.05 bar; (b) photographs of feed and permeate solutions after the filtration process.

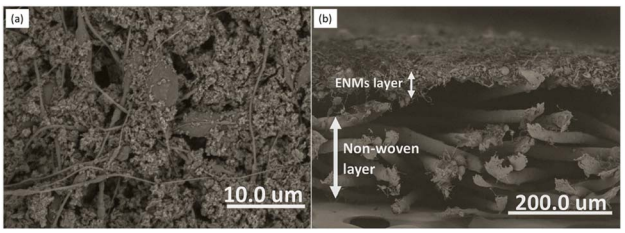


Fig. 11 SEM images of the first layer of ABSP1 ENMs after the filtration process and heating at 40 °C (a) filtered particles from surface view, and (b) cross-section view.

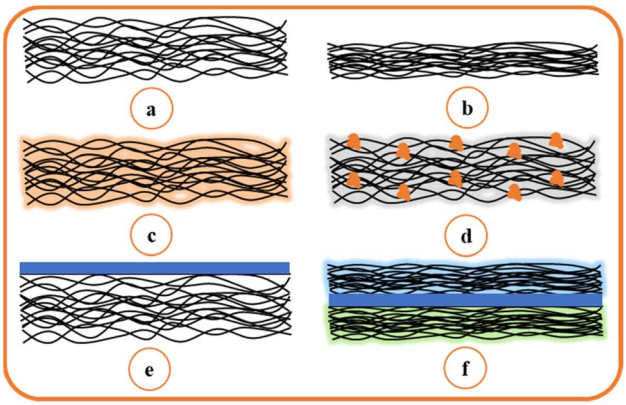


Fig. 12 Surface modification (a) normal nanofiber after synthesis, (b) heat treatment, (c) blending with other polymers or crosslinking, (d) incorporating with advanced powder materials, (e) layering the surface, (f) combining two types of modified nanofiber for advanced application.

clogging have been developed to enhance the reusability of the membranes. Latest studies to achieve surface filtration, remove a cake layer, and improve the mechanical and morphological properties are important contributions to minimizing the disadvantages.[77]

Based on this significant result, nanofiber membranes can be used in more advanced applications. However, challenges remain to make the membranes sufficiently strong, antifouling, and applicable to all types of waste treatment. The cake layer of pollutants in the nanofiber membranes is easy to remove and expected to render the membranes reusability. To restrict the pollutant on the surface, the nanofiber membranes should have a sufficiently strong surface to separate the pollutant. Fig. 12 depicts six types of surface modification methods in recent studies: (a) normal nanofiber synthesis, (b) heat treatment with annealing or direct warming at a specific temperature, (c) blending polymers with different properties or chemical crosslinking, (d) incorporating functional materials to obtain specific properties, (e) layering the nanofiber, and (f) combining two types of modified nanofiber.[83] The heat-annealed ENMs shown in Fig. 12(b) have several advantages, such as small pore size and excellent mechanical strength.[31,77] Blending with other copolymers makes the fiber more hydrophilic, and crosslinking with other materials can enhance the mechanical strength,[36,84] as shown in Fig. 12(c). Incorporating various functional material can achieve antibacterial, hydrophobic, and antifouling properties,[85–87] as shown in Fig. 12(d). The coating layer in Fig. 12(e) is usually made from water-soluble materials, enhancing the water flux and retaining the pollutant on the surface.[37] Furthermore, Fig. 12(f) is usually applied in membrane distillation applications, wherein two types of different polymers with modifications in each layer are incorporated; each layer can be heated to decrease the surface, crosslinked with other materials, or developed with a support layer.[88]

Table 2 compares the precursors, electrospinning parameters, ENMs characteristics, and efficiencies reported in the literature. Indeed, most of the published reports in Table 2 used non waste precursors to fabricate effective and high-performance nanofiber membranes. This study employed ABS waste to reduce the cost of the precursor and alleviate the environmental burden. As shown in Table 2, the fiber diameter in this study was comparable to that in other published reports. Moreover, compared with polylactic acid (PLA), polyether sulfones (PES), cellulose acetate (CA), polyimides (PI), and polysulfone (PSU) precursors with fiber diameters of 500–1700 nm, our study showed a reduced fiber diameter (108.46–216.64 nm). The rejection rate in this study was comparable to other ENMs, as shown in Table 2. Based on the comparison, nanofibers prepared by ABS waste with a simple PVP modification are suitable for the microfiltration process. This study provides a new strategy to reduce the amounts of WEEE in the environment, enhance the added value of recycled products and help to manage water resources. This result provides a promising way to utilize waste for more advanced membranes in the future.

Table 2 Published reports of electrospun nanofiber membranes in microfiltration[a]

| Precursor solution (polymer/solvent) | Electrospinning parameters concentration (wt%), voltage (kV), flow rate (mL $h^{-1}$), diameter needle tip (mm), collector distance (cm), humidity (%) | ENMs characteristics diameter (nm), porosity (%), water flux | Efficiency (%) |
|---|---|---|---|
| PAN/DMF[78] | 7–12, 18, 0.5, 0.4, NA, NA | 150–250, 34 to 86, 500–10 000 L $m^{-2}$ $h^{-1}$ | 99.3 |
| PLA/acetone[77] | 11–13, 20, 0.5, 0.4, 10, 30 | 500–1200, 5–70, 52 000–65 000 L $m^{-2}$ $h^{-1}$ | 10–85 |
| PAN-PET/DMF[32] | 4–18, 35, NA, 0.6, 7–19, 40 | 100–500, 61–74, 12 500–35 000 L $m^{-2}$ $h^{-1}$ | 93–99 |
| PES/NMP[31] | 25–40 w/v%, 10–15, 0.5, 1, 10–20, 50–60 | 550–1300, NA, 16 006 L $m^{-2}$ $h^{-1}$ $bar^{-1}$ | 100 |
| PVA/distilled water[79] | 10, 32, 0.6, 1, 10, 50–60 | 100–182, NA, ~5417 L $m^{-2}$ $h^{-1}$ $bar^{-1}$ | ~95 |
| CA/acetic acid–acetone[80] | 10, 10, 10 mL $h^{-1}$, 0.4, 15, NA | 500–1700, NA, 27 900 L $m^{-2}$ $h^{-1}$ $bar^{-1}$ | 87.7 |
| PAN/DMF[29] | 8–12, 20, 1.5–3, NA, 15, NA | 151–535, NA, 5000–7000 L $m^{-2}$ $h^{-1}$ | 81.4–99 |
| PI/NMP–xylene (4 : 1)[81] | 12, 16, 0.4, 0.4, NA, NA | <1000, NA, 514–17 607 L $m^{-2}$ $h^{-1}$ | 96.7 |
| PVA/citric acid–water (1 : 8)[30] | 10, 22, 2 μL $min^{-1}$, NA, 12/5, NA | 510–535, NA, 7500–13 500 L $m^{-2}$ $h^{-1}$ | 99 |
| PSU/DMF–THF (4 : 1)[82] | 20, 16, 2.5, 1.825, 10, 38–41 | 690–830, NA, NA | 75.3 |
| R-ABS-PVP/DMF (this study) | 28, 12, 0.3, 0.7, 12–15, 60 | 108.46–216.64, 64.18–71.78, 2951–48 041 L $m^{-2}$ $h^{-1}$ | 83–99 |

[a] PAN, polyacrylonitrile; PLA, polylactic acid; PES, polyether sulfones; PVA, polyvinyl alcohol; CA, cellulose acetate; PI, polyimides; PSU, polysulfone; NMP, *N*-methyl-2-pyrrolidone, THF tetrahydrofuran.

## Conclusions

ABS waste was successfully recycled as nanofiber membranes for microfiltration using an electrospinning technique. All the samples had similar characteristics, showing the presence of beads in the fiber. The average fiber diameter was 108.46–216.64 nm using a total 28 wt% ABS waste in DMF with a PVP concentration between 0 and 5 wt%. A high concentration of PVP (5 wt%) could decrease the number of beads, increase fiber diameter and surface porosity, also reduce WCA to achieve hydrophilic behavior. These properties influenced the performance of membrane filtration. The PWF was 2951–48 041 L $m^{-2}$ $h^{-1}$. A small amount of PVP (1 wt%) could enhance the rejection rate significantly from 83% (ABSP0) to 99% (ABSP1). This study emphasizes that polymeric waste could be a future material for inexpensive ENMs for advanced wastewater applications.

## Author contributions

Syarifa Nur'aini: formal analysis, methodology, investigation, writing – original draft. Akmal Zulfi: conceptualization, methodology, investigation, supervision, writing – review & editing. Bagas Haqi Arrosyid: formal analysis, investigation. Ande Fudja Rafriyanto: formal analysis, investigation. Alfian Noviyanto: conceptualization, formal analysis, supervision, funding acquisition, writing – review & editing. Dian Ahmad Hapidin: resources, supervision, writing – review & editing. Dafit Feriyanto: resources. Kurniawan Eko Saputro: formal analysis, resources. Khairurrijal: resources, writing – review & editing. Nurul T. Rochman: resources.

## Conflicts of interest

There are no conflicts to declare.

## Acknowledgements

This work was financially supported by the Kerjasama Dalam Negeri Scheme (KDN) [grant number 02-5/1082/B-SPK/III/2022], Mercu Buana University. The authors would like to express their gratitude to the Nano Center Indonesia for their facilities and characterization.

## References

1 D. M. Kulich, S. K. Gaggar, V. Lowry and R. Stepien, *Acrylonitrile–Butadiene–Styrene (ABS) Polymers*, John Wiley & Sons, Ltd, Hoboken, NJ, USA, 2003, vol. 1.
2 R. Balart, J. López, D. García and M. D. Salvador, *Eur. Polym. J.*, 2005, **41**, 2150–2160.
3 A. C. Ferreira, M. F. Diniz and E. da C. Mattos, *Polimeros*, 2018, **28**, 6–14.
4 J. Wang, Y. Li, J. Song, M. He, J. Song and K. Xia, *Polym. Degrad. Stab.*, 2015, **112**, 167–174.
5 R. Scaffaro, L. Botta and G. Di Benedetto, *Eur. Polym. J.*, 2012, **48**, 637–648.
6 P. Żur, A. Kołodziej, A. Baier and G. Kokot, *Eur. J. Eng. Sci. Technol.*, 1970, **3**, 44–51.
7 L. Gripon, I. Belyamani, B. Legros, K. Seaudeau-Pirouley, E. Lafranche and L. Cauret, *J. Waste Manage.*, 2021, **131**, 313–322.
8 L. Han, C. Chen, L. Shen, H. Lin, B. Li, Z. Huang, Y. Xu, R. Li and H. Hong, *J. Mater. Chem. A*, 2022, **10**, 12055–12061.
9 D. Vaes and P. Van Puyvelde, *Prog. Polym. Sci.*, 2021, **118**, 101411.
10 Z. Liu, Y. Wang, B. Wu, C. Cui, Y. Guo and C. Yan, *Int. J. Adv. Manuf. Technol.*, 2019, **102**, 2877–2889.
11 Y. Cui, Y. Li, W. Wang, X. Wang, J. Lin, X. Mai, G. Song, N. Naik and Z. Guo, *Sep. Purif. Technol.*, 2021, **269**, 118767.
12 T. D. Nguyen, T. M. Al Tahtamouni, P. T. Huong and P. Q. Thang, *J. Environ. Chem. Eng.*, 2019, **7**, 103354.
13 G. F. Cardamone, F. Ardolino and U. Arena, *J. Waste Manage.*, 2021, **126**, 119–132.
14 R. Al-Jarallah and E. Aleisa, *J. Waste Manage.*, 2014, **34**, 952–960.
15 H. Wang, X. L. Chen, Y. Bai, C. Guo and L. Zhang, *J. Waste Manage.*, 2012, **32**, 1297–1305.
16 C. Ma, J. Yu, B. Wang, Z. Song, J. Xiang, S. Hu, S. Su and L. Sun, *Renewable Sustainable Energy Rev.*, 2016, **61**, 433–450.
17 W. C. Qing, H. Wang, J. G. Fu and Y. N. Liu, *J. Waste Manage.*, 2015, **41**, 28–38.
18 P. K. Singh, S. K. Suman and M. Kumar, *Transp. Res. Procedia*, 2020, **48**, 3668–3677.
19 C. Areeprasert and C. Khaobang, *Fuel Process. Technol.*, 2018, **182**, 26–36.
20 M. I. Mohammed, A. Das, E. Gomez-Kervin, D. Wilson and I. Gibson, in *Solid Freeform Fabrication: Proceedings of the 28th annual international solid freeform fabrication symposium - an Additive Manufacturing Conference*, 2017, pp. 532–542.
21 A. Zulfi, D. A. Hapidin, M. M. Munir, F. Iskandar and K. Khairurrijal, *RSC Adv.*, 2019, **9**, 30741–30751.
22 M. M. Munir, A. I. Kamil and M. Burhanuddin, *J. Mater. Res. Technol.*, 2022, **18**, 4564–4577.
23 R. Sarbatly, J. Sariau and M. F. I. Alam, *Mater. Today Proc.*, 2021, **46**, 2118–2121.
24 S. Agrawal, R. Ranjan, B. Lal, A. Rahman, S. P. Singh, T. Selvaratnam and T. Nawaz, *Processes*, 2021, **9**, 1779.
25 M. Khraisheh, S. Elhenawy, F. Almomani, M. Al-Ghouti, M. K. Hassan and B. H. Hameed, *Membranes*, 2021, **11**, 995.
26 Z. Uddin, F. Ahmad, T. Ullan, Y. Nawab, S. Ahmad, F. Azam, A. Rasheed and M. S. Zafar, *Int. J. Environ. Sci. Technol.*, 2022, **19**, 9149–9176.
27 S. S. Ray, S. S. Chen, C. W. Li, N. C. Nguyen and H. T. Nguyen, *RSC Adv.*, 2016, **6**, 85495–85514.
28 N. S. Abd Halim, M. D. H. Wirzal, S. M. Hizam, M. R. Bilad, N. A. H. M. Nordin, N. S. Sambudi, Z. A. Putra and A. R. M. Yusoff, *J. Environ. Chem. Eng.*, 2021, **9**, 104613.
29 T. Aslan, S. Arslan, M. Eyvaz, S. Güçlü, E. Yüksel and İ. Koyuncu, *J. Memb. Sci.*, 2016, **520**, 616–629.
30 E. Karimi, A. Raisi and A. Aroujalian, *Polymer*, 2016, **99**, 642–653.
31 J. Bae, I. Baek and H. Choi, *Water Res.*, 2016, **105**, 406–412.

32 S. M. Seyed Shahabadi, S. A. Mousavi and D. Bastani, *J. Taiwan Inst. Chem. Eng.*, 2016, **76**, 474–483.
33 A. Mamun, T. Blachowicz and L. Sabantina, *Polymers*, 2021, **13**, 1–14.
34 S. Jiang, H. Schmalz, S. Agarwal and A. Greiner, *Adv. Fiber Mater.*, 2020, **2**, 34–43.
35 S. Kumarage, I. Munaweera and N. Kottegoda, *Beilstein J. Nanotechnol.*, 2022, **13**, 137–159.
36 Y. Wu, J. Zeng, Y. Zeng, H. Zhou, G. Liu, J. Jian and J. Ding, *Chin. J. Chem. Eng.*, 2021, **38**, 84–97.
37 M. J. Park, R. R. Gonzales, A. Abdel-Wahab, S. Phuntsho and H. K. Shon, *Desalination*, 2018, **426**, 50–59.
38 M. Abdullah and K. Khairurrijal, *Indones. J. Phys.*, 2016, **20**, 37–40.
39 C. D. Tsakiroglou, M. A. Ioannidis, E. Amirtharaj and O. Vizika, *Chem. Eng. Sci.*, 2009, **64**, 847–859.
40 A. Sawitri, M. M. Munir, D. Edikresnha, A. Sandi, A. Fauzi, A. Rajak, D. Natalia and K. Khairurrijal, *Mater. Res. Express*, 2018, **5**, 54003.
41 R. Wang, Y. Liu, B. Li, B. S. Hsiao and B. Chu, *J. Memb. Sci.*, 2012, **392–393**, 167–174.
42 K. Oshvandi, R. Kavyannejad, R. S. Borzuo and M. Gholyaf, *Nurs. Midwifery Stud.*, 2014, **3**, e21764.
43 S. R. Selvi and R. Baskaran, in *APCBEE Procedia*, Elsevier BV, 2014, vol. 9, pp. 97–101.
44 T. Mudalige, H. Qu, D. Van Haute, S. M. Ansar, A. Paredes and T. Ingle, *Nanomater. Food Appl.*, 2019, 313–353.
45 R. Gopal, S. Kaur, Z. Ma, C. Chan, S. Ramakrishna and T. Matsuura, *J. Membr. Sci.*, 2006, **281**, 581–586.
46 K. M. Dobosz, C. A. Kuo-Leblanc, T. J. Martin and J. D. Schiffman, *Ind. Eng. Chem. Res.*, 2017, **56**, 5724–5733.
47 Y. Liu, L. Shen, Z. Huang, J. Liu, Y. Xu, R. Li, M. Zhang, H. Hong and H. Lin, *J. Membr. Sci.*, 2022, **641**, 119925.
48 A. Rajak, D. A. Hapidin, F. Iskandar, M. M. Munir and K. Khairurrijal, *J. Waste Manage.*, 2020, **103**, 76–86.
49 H. Sanaeepur, A. Ebadi Amooghin, A. Moghadassi, A. Kargari, S. Moradi and D. Ghanbari, *Polym. Adv. Technol.*, 2012, **23**, 1207–1218.
50 I. N. Strain, Q. Wu, A. M. Pourrahimi, M. S. Hedenqvist, R. T. Olsson and R. L. Andersson, *J. Mater. Chem. A*, 2015, **3**, 1632–1640.
51 M. Gu, K. Wang, W. Li, C. Qin, J. J. Wang and L. Dai, *Fibers Polym.*, 2011, **12**, 65–72.
52 R. Kumar, R. Singh and I. Farina, *PSU Res. Rev.*, 2018, **2**, 115–137.
53 J. Lv, W. Gu, X. Cui, S. Dai, B. Zhang and G. Ji, *Sci. Rep.*, 2019, **9**, 1–11.
54 I. Turku, S. Kasala and T. Kärki, *Recycling*, 2018, **3**, 57.
55 G. Liu, Y. Liao and X. Ma, *J. Waste Manage.*, 2017, **61**, 315–326.
56 A. Fauzi, D. A. Hapidin, M. M. Munir, F. Iskandar and K. Khairurrijal, *RSC Adv.*, 2020, **10**, 17205–17216.
57 E. Moradi, H. Ebrahimzadeh and Z. Mehrani, *Talanta*, 2019, **205**, 120080.
58 B. Ozbey-Unal, E. Gezmis-Yavuz, B. Eryildiz, D. Y. Koseoglu-Imer, B. Keskinler and I. Koyuncu, *J. Environ. Chem. Eng.*, 2020, **8**, 104113.
59 J. Matulevicius, L. Kliucininkas, T. Prasauskas, D. Buivydiene and D. Martuzevicius, *J. Aerosol Sci.*, 2016, **92**, 27–37.
60 M. Borrego, J. E. Martín-Alfonso, M. C. Sánchez, C. Valencia and J. M. Franco, *Int. J. Biol. Macromol.*, 2021, **180**, 212–221.
61 I. Sriyanti, D. Edikresnha, A. Rahma, M. M. Munir, H. Rachmawati and K. Khairurrijal, *J. Nanomater.*, 2017, **2017**, 9687896.
62 W. T. Kim, D. C. Park, W. H. Yang, C. H. Cho and W. Y. Choi, *Nanomaterials*, 2021, **11**, 26–28.
63 A. A. Almetwally, M. El-Sakhawy, M. H. Elshakankery and M. H. Kasem, *J. Text. Assoc.*, 2017, **78**, 5–14.
64 Y. Liu, J. H. He, J. Y. Yu and H. M. Zeng, *Polym. Int.*, 2008, **57**, 632–636.
65 S. Higashi, T. Hirai, M. Matsubara, H. Yoshida and A. Beniya, *Sci. Rep.*, 2020, **10**, 13427.
66 Z. Huang, L. Shen, H. Lin, B. Li, C. Chen, Y. Xu, R. Li, M. Zhang and D. Zhao, *J. Membr. Sci.*, 2022, **661**, 120949.
67 I. M. Alarifi, A. R. Alharbi, M. Khan, W. S. Khan, A. Usta and R. Asmatulu, *Int. J. Mater. Sci. Res.*, 2018, **2**, 43–49.
68 A. Gençtürk, E. Kahraman, S. Güngör, Y. Özsoy and A. S. Saraç, *Turkish J. Pharm. Sci.*, 2020, **17**, 638–644.
69 I. Tlili and T. A. Alkanhal, *J. Water Reuse Desalin.*, 2019, **9**, 232–247.
70 A. Atangana, in *Fractional Operators with Constant and Variable Order with Application to Geo-Hydrology*, Academic Press, 2018, pp. 15–47.
71 K. Damak, A. Ayadi, B. Zeghmati and P. Schmitz, *Desalination*, 2004, **161**, 67–77.
72 Z. Zhou and X. F. Wu, *Mater. Lett.*, 2015, **160**, 423–427.
73 A. Zulfi, M. M. Munir, D. A. Hapidin, A. Rajak, D. Edikresnha, F. Iskandar and K. Khairurrijal, *Mater. Res. Express*, 2018, **5**, 035049.
74 O. Abdalla, M. A. Wahab and A. Abdala, *Curr. Pharm. Biotechnol.*, 2020, **22**, 1686–1704.
75 N. Zhou, R. Liang and A. Hu, *Nanotechnology for water treatment and purification*, Springer International Publishing, Switzerland, 2014, vol. 22.
76 L. Bao, K. Seki, H. Niinuma, Y. Otani, R. Balgis, T. Ogi, L. Gradon and K. Okuyama, *Sep. Purif. Technol.*, 2016, **159**, 100–107.
77 L. Li, R. Hashaikeh and H. A. Arafat, *J. Membr. Sci.*, 2013, **436**, 57–67.
78 Z. Wang, C. Crandall, R. Sahadevan, T. J. Menkhaus and H. Fong, *Polymer*, 2017, **114**, 64–72.
79 Y. Liu, R. Wang, H. Ma, B. S. Hsiao and B. Chu, *Polymer*, 2013, **54**, 548–556.
80 L. A. Goetz, B. Jalvo, R. Rosal and A. P. Mathew, *J. Membr. Sci.*, 2016, **510**, 238–248.
81 A. K. Gautam, C. Lai, H. Fong and T. J. Menkhaus, *J. Membr. Sci.*, 2014, **466**, 142–150.
82 P. Arribas, M. C. García-Payo, M. Khayet and L. Gil, *Sep. Purif. Technol.*, 2019, **226**, 323–336.
83 H. Saleem, L. Trabzon, A. Kilic and S. J. Zaidi, *Desalination*, 2020, **478**, 114178.

84 E. F. C. Chaúque, L. N. Dlamini, A. A. Adelodun, C. J. Greyling and J. C. Ngila, *Phys. Chem. Earth*, 2017, **100**, 201–211.
85 X. Yin, Y. He, Y. Wang, H. Yu, J. Chen and Y. Gao, *Korean J. Chem. Eng.*, 2020, **37**, 1751–1760.
86 S. Hartati, A. Zulfi, P. Y. D. Maulida, A. Yudhowijoyo, M. Dioktyanto, K. E. Saputro, A. Noviyanto and N. T. Rochman, *ACS Omega*, 2022, **7**, 10516–10525.
87 X. Wang, L. Zhai, Y. Wang, R. Li, X. Gu, Y. Di Yuan, Y. Qian, Z. Hu and D. Zhao, *ACS Appl. Mater. Interfaces*, 2017, **9**, 37848–37855.
88 T. Zhou, J. Li, X. Guo, Y. Yao, P. Zhu and R. Xiang, *Desalin. Water Treat.*, 2019, **165**, 63–72.